

Changes in Pore Characteristics of Alkali-activated Slag Paste after Freeze-thaw Cycles

Yin Xueqian¹, Liu Lin^{1,2,a}, Dai Haoyu¹ and Qin Sainan¹

¹ Jiangsu Engineering Research Center of Concrete Cracking, College of Civil and Transportation Engineering, Hohai University, Nanjing 210098, China

² Jiangsu Research Institute of Building Science Co., LTD., Nanjing 210008, China

^aliulin@hhu.edu.cn

Abstract. The freeze-thaw resistance of Alkali-activated slag (AAS) material is one of its important properties when applied in cold areas, which is intrinsically related to its pore structure. In order to investigate changes in the pore characteristics of AAS paste subjected to freeze-thaw action, AAS paste samples after different freeze-thaw cycles (i.e., 0, 3, 9, 15 cycles) are tested by low temperature calorimetry (LTC). From the baselines obtained by recording the heat flow of the AAS pastes at different testing temperatures, it is found that no matter in the freezing or melting process, the maximum heat flow-jump increased with the increasing freeze-thaw cycles. From the ice content with temperature change, it is found that the ice in pores mainly melts in the temperature range of -5 °C to 0 °C, and the more freeze-thaw cycles the sample suffered, the more ice melted in this temperature range. The pore structure were coarsened by freezing/thawing, demonstrated by the volume of pores within 8-100 nm increased with the increasing freeze-thaw cycles, and the main increase of pore volume caused by freeze-thaw cycles is in the range of 50-100 nm.

1. Introduction

Alkali-activated slag (AAS) is a new type of cementitious material developed in recent decades which is made from Ground Granulated Blast Furnace Slag (GGBFS) and alkaline solution. Compared with ordinary Portland cement (OPC), AAS has lower carbon dioxide emission, less energy and materials consumption, better mechanical properties and durability [1].

The freeze-thaw resistance of AAS is one of the most important properties when it is applied in the cold areas. Ellis et al. made AAS with KOH solution and freeze-thaw testing up to 100 freeze-thaw cycles was performed in 10% road salt solution, it is found that compressive strength of up to 100 MPa after 28 days of curing and 120 MPa after freeze-thaw testing [2]. Fu et al. studied the freeze-thaw resistance and hydration products of alkali-activated slag concrete, the experimental results show that it has excellent freeze-thaw resistance with frost-resisting grade of F300 at lowest; hydration products are mostly C-S-H(I) with low Ca/Si, alkaline aluminosilicate and zeolite mineral, no Ca(OH)₂ and ITZ; its compact and homogeneous structure and high compressive strength makes high freeze-thaw resistance [3]. Cai et al. analyzed freeze-thaw resistance of alkali-activated slag concrete based on response surface methodology and found that the influence on the freeze-thaw resistance from high to low is Ca/Si, slag content and sand ratio [4].

In Portland cement based materials, it has been shown that the properties that effect freeze-thaw resistibility are mostly physicomechanical properties like pore structure, pore saturation and entrained air voids, it is thought that this relationship may be similar for alkali-activated materials [1].



Researches on pore structure of AAS have been done [5-12] and some common conclusions have been proposed. The pore size distribution of slag-OPC blended cements becomes finer with increasing slag content [5,6]. In the case of AAS, the proportion of pores in the micropore size range tend to be higher than OPC [7,8], the proportion of pore sizes within the mesopore is much higher than OPC [9,10], the number of pores within the capillary range is lower than OPC [11,12]. Research on pore structures helps us essentially understand the frost damage mechanism, therefore, it is of significance to study the pore structure evolution of AAS in freeze-thaw cycles. However, rare studies have been carried out in the pore structure changes of AAS after freeze-thaw cycles.

Compared with traditional methods (e.g., NAD, MIP and SEM) developed for pore characterization, a major advantage of using low temperature calorimetry (LTC) is that the measurements can be conducted on virgin samples without pre-drying treatment [13]. This is important because the drying treatment often results in an apparent alteration of the pore structure under consideration for cement based materials [14]. Previous studies have shown good applicability of LTC in cement based materials, but it should be referred that water in very small pores does not freeze and the freezing/melting point depression of water/ice in big pores is too small. Therefore, the pores that can presented well by LTC are those with radii between about 2-50 nm [13]. Since the mesopores are predominant in pore structure of AAS materials, the LTC method would be an appropriate way to investigate pore structure of AAS.

In order to understand the influence of freeze-thaw cycles on pore structure of AAS, pore characteristics of AAS paste after freeze-thaw cycles are tested by LTC. AAS pastes after 0, 3, 9, and 15 freeze-thaw cycles are first prepared. Then, the freezing and melting heat flow of samples at different test temperatures is recorded. Next, the ice content and the pore size distribution of the AAS pastes are calculated by analyzing the heat flow data.

2. Materials and experiment

2.1. Materials

The raw materials used in this study is GGBFS, its chemical compositions are listed in Table 1.

Sodium metasilicate nonahydrate ($\text{Na}_2\text{SiO}_3 \cdot 9\text{H}_2\text{O}$) was used as alkali activator, module of the activator (molar ratio of $\text{SiO}_2/\text{Na}_2\text{O}$) is 1.03 ± 0.03 .

Table 1. Composition of the GGBFS (mass% as oxide)

CaO	SiO ₂	Al ₂ O ₃	MgO	S	TiO ₂	K ₂ O	Fe ₂ O ₃	MnO	Na ₂ O
37.17	33.23	17.76	7.53	1.24	0.992	0.531	0.416	0.404	0.311

2.2. Sample preparation

AAS pastes were formulated with a constant water/binder (slag + Na_2SiO_3) ratio of 0.4. The dosage of alkaline activator was 8 g Na_2SiO_3 per 100 g of slag ($\text{Na}_2\text{O}_{\text{eq}} = 4.1\%$). These solid activators were dissolved into mixing water first and then added to the slag during the paste mixing. After mixing, the pastes were cast in cylindrical mold of 20 mm in diameter and cured at a relative humidity of $60 \pm 5\%$ and a temperature of 20 ± 3 °C for 14 days under sealed condition. Then the AAS pastes were sawn into disk-like samples with a thickness of 2 mm for freeze-thaw cycles.

Tests of AAS samples exposed to freeze-thaw cycles were carried out in a programmable temperature and humidity chamber. The cycle temperature is +4 °C to -30 °C, 16 h per cycle, freezing from +4 °C to -30 °C for 4 h, keeping in -30 °C for 4 h, thawing from -30 °C to +4 °C for 4 h, and keeping in +4 °C for 4 h. Four samples suffered 0, 3, 9 and 15 freeze-thaw cycles were prepared.

2.3. LTC test

After specific freeze-thaw cycles, the samples were broken into small pieces of 20-30 mg and immersed in saturated sodium hydroxide solution till LTC test. Four groups of samples was tested to

reveal the pore structure evolution of AAS pastes subjected to freeze-thaw cycles, and the samples were assumed that they were fully saturated before test.

To minimize the temperature lag between the instrument and the samples, a drop of kerosene was added on top of the samples to improve thermal contact with the aluminum sample pan and to minimize drying of the samples while the lid was being crimped onto the pan [13]. By using NETZSCH DSC 214 Differential Scanning Calorimeter, the samples were subjected to heating and cooling cycle over the range from +5 °C to -40 °C at a rate of 1 °C/min, and the heat flow of the samples at different testing temperatures were recorded.

3. Result and discussion

3.1. Interpretation of LTC data

Generally, the baseline of heat flow obtained by LTC test will slightly change during the temperature changing, and there will be obvious upwards movement when water transforms into ice and downwards when ice transforms into water. There are two methods of calculating the baseline and the ice content, called “J-baseline” method [15] and “C-baseline” method [13]. The “C-baseline” method was employed in this paper.

The experimental data were taken at a small temperature interval, ΔT , so the mass of ice m_C at a certain temperature step can be obtained following the “C-baseline” method [13],

$$m_C(T + \Delta T) \approx \left[m_C(T) + \frac{\Delta T}{2} \left(\frac{Q(T) - Q_0}{qh_f} \right) \right] \times \exp \left[\frac{(C_{PC} - C_{PL})\Delta T}{h_f} \right] + \frac{\Delta T}{2} \left(\frac{Q(T + \Delta T) - Q_0}{qh_f} \right) \quad (1)$$

Q_0 (unit: mW) represents the heat flow at the point where the water starts to freeze (right before the first peak observed on a measured heat flow curve during freezing); and $Q(T)$ (unit: mW) represents the heat flow at temperature T (unit: °C) measured by LTC. q (unit: °C/s) and h_f (unit: J/g) represent the corresponding cooling/heating rate and the heat of fusion. The heat of fusion (unit: J/g) in the freezing was adopted as $h_f = 332.4$ and that in melting was adopted as $h_f = 333.8 + 1.797(T - T_M)$, where T_M (unit: °C) is the melting temperature of bulk ice [13]. C_{PC} and C_{PL} (unit: J/(g·K)) represent the heat capacity of ice and water respectively. The heat capacity of water and ice are proved to be not very sensitive to temperature; therefore, 4.2176 J/(g·K) for water and 2.114 J/(g·K) for ice were adopted [16]. It should be noted that the baseline for the freezing and the melting processes almost always are found to be different, due to the hysteresis effect in the freezing and melting process. Equation (1) can also be employed if we analyze the melting process inversely from the high to the low temperature end and treat the data similar to a “freezing process”. The Q_0 would then be the heat flow after all of the ice has been melted [16].

After the mass of ice formed or melted in each temperature interval was obtained, the volume of ice $\Delta V_C(\Delta T)$ (unit: cm³) can be calculated by dividing by the density of ice, $\rho_C(T)$ (unit: g/cm³) [17],

$$\Delta V_C(\Delta T) = \frac{m_C(T + \Delta T) - m_C(T)}{\rho_C(T)} \quad (2)$$

$$\rho_C(T) \approx 0.9167 - 2.053 \times 10^{-4} T - 1.357 \times 10^{-6} T^2 \quad (3)$$

There is an unfrozen layer of water with thickness δ , so the radius of the pore, r_p (unit: nm), is related to the radius of the ice crystal r_{CL} by $r_p = r_{CL} + \delta$. Based on comparisons of MIP and thermoporometry results for various porous materials, Brun et al. concluded that $\delta = 0.8$ nm for water [18]. The expression for r_{CL} (unit: nm) as a function of ΔT in freezing is [13]

$$r_{CL} = \frac{64.67}{\Delta T} - 0.23 \quad (4)$$

during the melting, the function is

$$r_{CL} = \frac{32.33}{\Delta T} + 0.11 \quad (5)$$

The volume of the pores in which freezing occurs, v_{pore} (unit: cm^3), is greater than the volume of the ice v_{ice} (unit: cm^3) by a factor of [13]

$$v_{\text{pore}} = v_{\text{ice}} \left(\frac{r_{\text{CL}} + \delta}{r_{\text{CL}}} \right)^n \quad (6)$$

where $n = 2$ for a cylindrical pore and $n = 3$ for a spherical pore.

By following the “C-baseline” method introduced above, the tested baselines for the freezing and melting processes of AAS pastes of different freeze-thaw cycles could be analyzed to calculate the ice content and the pore size distribution.

3.2. Baselines

The tested baselines of the AAS pastes in the freezing and melting are shown in Figure 1.

Figure 1(a) illustrates that the more freeze-thaw cycles, the larger maximum heat flow-jump. It indicates that more ice is formed after the nucleation point with the increasing freeze-thaw cycles. For the freezing process, ice doesn't form immediately at the freezing point T_M where bulk ice in the air can be formed. Ice nucleates at a supercooled state, and the heat flow jumped sharp indicates a large amount of ice formed after nucleation due to the supercooling. As to the melting process in Figure 1(b), the more freeze-thaw cycles, the larger maximum heat flow-jump too, but jump downwards.

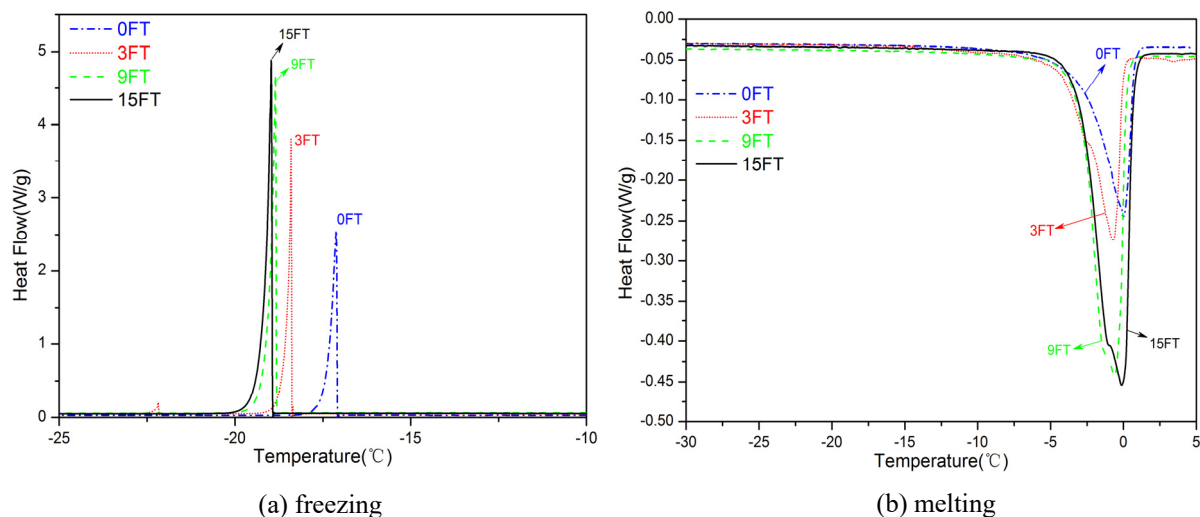


Figure 1. Baselines for the freezing and melting process of AAS pastes of different F-T cycles

3.3. Ice content and pore size distribution

The freezing curve is related to the characteristics of pore entry size, while the melting curve is related to the characteristics of pore interior size [13]. Thus the melting process is usually employed to analyze ice content and pore size distribution. According to the “C-baseline” method, the ice content during melting process is shown in Figure 2. It shows that the ice content decreases with the increasing temperature during melting process for each sample. It shows that the ice in pores of the AAS pastes mainly melts in the temperature range of $-5\text{ }^{\circ}\text{C}$ to $0\text{ }^{\circ}\text{C}$, the more the freeze-thaw cycles, the more the ice melted in this temperature range.

Based on the relationship between the pore radius and the temperature during freezing or melting, the pore size distribution of the pastes is obtained. The data of pore size within 8-100 nm range is discussed in consideration of the suitable range of LTC, the cumulative pore volume from pore size 100 nm to 8 nm is shown in Figure 3. It demonstrates the influence of freeze-thaw cycles on the pore structure of the AAS pastes, the results shows that cumulative pore volume of the samples increased with the increasing freeze-thaw cycles. In the range of 50-100 nm, it is obvious that the pore volume increasing gradually in the case of 0 cycle, then the increase of pore volume become sharp with

increasing freeze-thaw cycles, which means the increase of pore volume caused by freeze-thaw cycles mainly in the range of 50-100 nm.

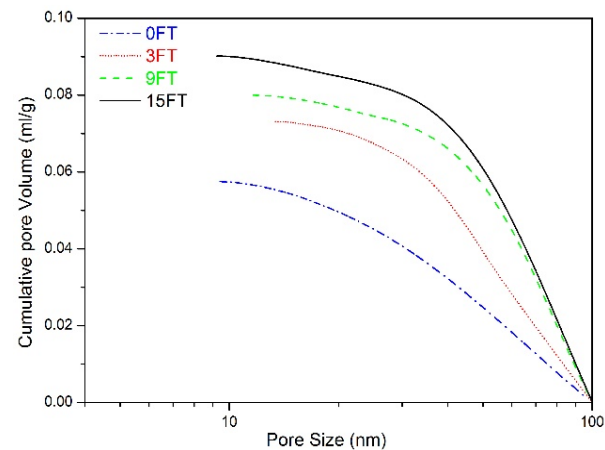
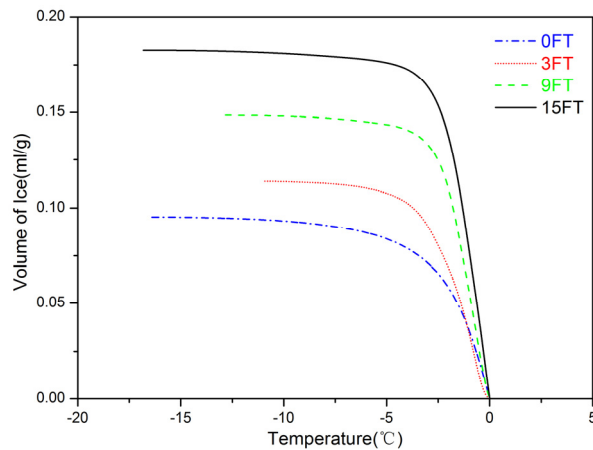


Figure 2. Volume of ice versus temperature

Figure 3. Pore size distribution between 8-100 nm

The frost resistance of paste is associated with the porosity and pore size distribution of the paste, lower porosity and finer pore size distribution usually leads to higher frost resistance, and the pore structure of paste is effected by freeze-thaw cycles. Figure 4 gives the classified pore volume proportion of AAS pastes which diameter within 8-50 nm, 50-100 nm, and above 100 nm. It should be noted that water in large pores (with pore size larger than 100 nm) still can be monitored by LTC, but due to the small difference in freezing temperature depression between large pores, the pore size distribution is not accurate. However, the total pore volume for pores larger than 100 nm can be utilized. It shows that with the increase of freeze-thaw cycles, pores in 8 - 50 nm (i.e., mesopores) tend to be less, while pores in 50-100 nm and above 100 nm (i.e., macropores) tend to be more. So after the freeze-thaw cycles, the small pores become large pores. That is to say, the pore size of the AAS pastes tends to be larger and the pore size distribution become coarser with the increasing freeze-thaw cycles.

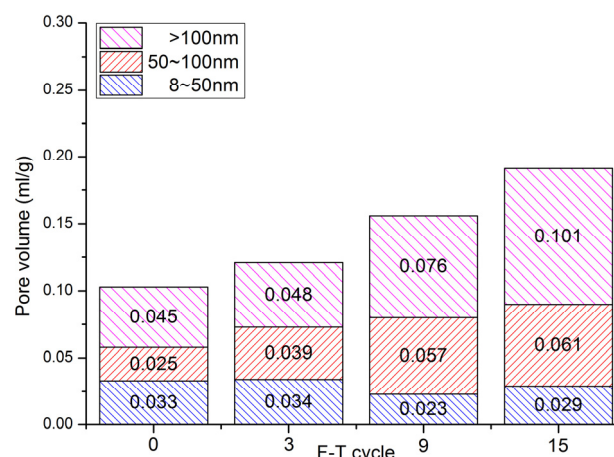


Figure 4. Classified pore volume proportion of the AAS pastes with different freeze-thaw cycles

4. Conclusions

This paper investigated the changes in pore characteristics of AAS paste after freeze-thaw cycles by LTC. From the test results and data analysis, the following conclusions can be drawn:

- The baselines obtained by recording the heat flow of the AAS pastes at different testing temperatures shows that the maximum heat flow-jump of the pastes increased with the increasing freeze-thaw cycles no matter in the freezing or melting process.

- From the ice content with temperature change, it is found that the ice in pores of the AAS pastes mainly melts in the temperature range of -5 °C to 0 °C, and the more the freeze-thaw cycles, the more ice melted in this temperature range.
- The pore structure of AAS pastes were coarsened by freezing/thawing, demonstrated by the volume of pores within 8-100 nm increased with the increasing freeze-thaw cycles, and the main increase of pore volume caused by freeze-thaw cycles is in the range of 50-100 nm.

Acknowledgements

The financial supports of National Natural Science Foundation of China via Grant No.51678219, General Financial Grant and Special Financial Grant from the China Postdoctoral Science Foundation via Grant No.2016M590428 & No.2017T100339 are greatly acknowledged.

References

- [1] Provis J L, Deventer J S J V 2014 *Alkali Activated Materials* (Berlin: Springer)
- [2] Ellis K, Alharbi N, Matheu P S, Varela B and Hailstone R 2015 Durability of Alkali Activated Blast Furnace Slag *IOP Conf. Ser. Mater. Sci. Eng.* Vol 96 p 012004
- [3] Fu Y, Cai L and Wu Y 2011 Freeze-thaw cycle test and damage mechanics models of alkali-activated slag concrete *Construction & Building Materials* **25** 3144-48
- [4] Cai L, Wang H and Fu Y 2013 Freeze-thaw resistance of alkali-slag concrete based on response surface methodology *Construction & Building Materials* **49** 70-76
- [5] Gjorv O E and Ø Vennesland 1979 Diffusion of chloride ions from seawater into concrete *Cement & Concrete Research* **9** 229-238
- [6] Mehta P K 1987 Pozzolanic and cementitious byproducts as mineral admixtures for concrete – a critical review *Journal of the American Concrete Institute* **80** 340-340
- [7] Hakkinen T 1992 The microstructure of high strength blast furnace slag concrete *NORDIC CONCRETE RESEARCH. PUBLICATION NO 11*
- [8] Häkkinen T 1993 The influence of slag content on the microstructure, permeability and mechanical properties of concrete : part 2 technical properties and theoretical examinations *Cement & Concrete Research* **23** 518-530
- [9] Collins F and Sanjayan J G 2000 Effect of pore size distribution on drying shrinking of alkali-activated slag concrete *Cement & Concrete Research* **30** 1401-06
- [10] Collins F and Sanjayan J G 2001 Microcracking and strength development of alkali activated slag concrete *Cement & Concrete Composites* **23** 345-352
- [11] Malolepszy J and Deja J K 2011 Effect of heavy metals immobilization on the properties of alkali activated slag mortars *Journal of Materials in Civil Engineering* **23** 886-894
- [12] Deja J and Malolepszy J 1989 Resistance of alkali-activated slag mortars to chloride solution *Aci Special Publication* **114** 1547-64
- [13] Sun Z and Scherer G W 2010 Pore size and shape in mortar by thermoporometry *Cement & Concrete Research* **40** 740-751
- [14] Espinosa R M and Franke L 2006 Influence of the age and drying process on pore structure and sorption isotherms of hardened cement paste *Cement & Concrete Research* **36** 1969-84
- [15] Johannesson B 2010 Dimensional and ice content changes of hardened concrete at different freezing and thawing temperatures *Cement & Concrete Composites* **32** 73-83
- [16] Wu M, Johannesson B & Geiker M 2014 Determination of ice content in hardened concrete by low-temperature calorimetry *Journal of Thermal Analysis & Calorimetry* **115** 1335-51
- [17] Lide D 2003 *Crc handbook of chemistry and physics* (Florida: Crc Press) p 423
- [18] Brun M, Lallemand A, Quinson J F & Eyraud C 1977 A new method for the simultaneous determination of the size and shape of pores: the thermoporometry *Thermochimica acta* **21** 59-88